

CHEMICAL POTENTIAL DEPENDENCE OF PARTICLE RATIOS WITHIN A UNIFIED THERMAL APPROACH

*I. Bashir**, *H. Nanda*, *S. Uddin*

*Department of Physics, Jamia Millia Islamia (Central University)
110025, New-Delhi, India*

Received September 19, 2015

A unified statistical thermal freeze-out model (USTFM) is used to study the chemical potential dependence of identified particle ratios at mid-rapidity in heavy-ion collisions. We successfully reproduce the experimental data ranging from SPS energies to LHC energies, suggesting the statistical nature of the particle production in these collisions and hence the validity of our approach. The behavior of the freeze-out temperature is studied with respect to chemical potential. The freeze-out temperature is found to be universal at the RHIC and LHC and is close to the QCD predicted phase transition temperature, suggesting that the chemical freeze-out occurs soon after the hadronization takes place.

DOI: 10.7868/S0044451016060080

1. INTRODUCTION

Statistical thermal models have successfully reproduced the essential features of particle production in heavy-ion collisions [1] as well as in many types of elementary collisions [2]. Systematic studies of particle yields using experimental results at different beam energies have revealed a clear underlying freeze-out pattern for particle yields in heavy-ion collisions [3]. The success of the statistical (thermal) models in describing the ratios of hadron yields produced in heavy ion collisions is remarkable. The agreement of the particle ratios with simple predictions of the statistical models is a key argument for the thermalization of the system formed in heavy-ion collisions. Measurements of antiparticle-to-particle ratios in these collisions give information on the net baryon density or baryon chemical potential achieved and are therefore of interest in characterizing the environment created in these collisions. It has also been suggested that the measurement of strange antibaryon-to-baryon ratios could help distinguish between a hadron gas and a deconfined plasma of quarks and gluons [4]. For a boost-invariant system at mid-rapidity for the RHIC and LHC energies, the particle yields dN/dy change only by a few percent in the rapidity window $|y| < 1$, thus giving a plateau-like distribution within this rapidity interval. Although the

particles detected at mid-rapidity are collected from various parts of the fireball, their ratios are the same as in the 4π calculations. This holds even when the resonance decay contributions are included.

In this paper, we attempt to reproduce the particle ratios and to study their dependence on the mid-rapidity chemical potential in the hadronic gas scenario by using our phenomenological boost-invariant unified statistical thermal freeze-out model (USTFM) [5], which assumes that at freeze-out, all the hadrons in the hadron gas resulting from a high-energy nuclear collision follow an equilibrium distribution. The local particle phase-space densities have the form of the Fermi–Dirac or Bose–Einstein statistical distributions. The momentum distributions of hadrons emitted from within an expanding fireball and assumed to be in the state of local thermal equilibrium are characterized by the Lorentz-invariant Cooper–Frye formula

$$E \frac{d^3n}{d^3p} = \frac{g}{(2\pi)^3} \int f \left(\frac{p^\mu u^\mu}{T}, \lambda \right) p^\mu d\Sigma_\mu, \quad (1)$$

where Σ_f represents a 3-dimensional freeze-out hypersurface, g is the degeneracy factor of a given hadronic species in the expanding relativistic hadronic gas and is only determined by the degrees of freedom of the given hadron, λ is the fugacity $\exp(\mu/T)$ of the given hadronic species, μ is the chemical potential, and u^μ is the flow velocity, which, in general, depends on space and time. In this approach, unlike in the other thermal models that take a single value of the chemical potential μ_B for the fireball produced in the collision

* E-mail: inamhep@gmail.com

process, we have chosen a varying rapidity-dependent baryonic chemical potential μ_B written in the form

$$\mu_B = a + by_0^2, \quad (2)$$

where y_0 is the rapidity of the expanding hadronic fluid element along the beam axis (z axis). This is because a strong evidence of the increasing baryon chemical potential along the rapidity axis has been found in [6]. Here, a and b are the two model parameters, which can be fixed by fitting the experimental data. In the model, the value of a essentially defines the baryon chemical potential in the central region (mid-rapidity) of the bulk hadronic matter formed, and b determines the rate of increase of the baryon chemical potential along the (longitudinal) rapidity axis with y_0 . The rapidity of the expanding hadronic fluid element is $y_0 \propto z$ or $y_0 = cz$, where z is the longitudinal coordinate of the hadronic fluid element and c is a proportionality constant. The above conditions also ensure that under the transformation $z \rightarrow -z$, we have $y_0 \rightarrow -y_0$, thereby preserving the symmetry of the hadronic fluid flow about $z = 0$ along the rapidity axis in the center-of-mass frame of the colliding nuclei. Unlike in case of the blast wave model, where a common radial flow velocity is assumed for the emitted particles, we in this model take the longitudinal as well as the transverse components of the hydrodynamic flow into account. The longitudinal velocity component of the hadronic fluid element is written as

$$\beta_z(z) = 1 - \frac{2}{\exp(2cz) + 1} = \tanh y_0. \quad (3)$$

The transverse velocity component of the hadronic fireball β_T is assumed to vary with the transverse coordinate r in accordance with the blast wave model as [5]

$$\beta_T(r) = \beta_T^s \left(\frac{r}{R} \right)^n, \quad (4)$$

where n is an index that determines the profile of $\beta_T(r)$ and β_T^s is the hadronic fluid surface transverse expansion velocity and is fixed in the model by using the parameterization [5]

$$\beta_T^s = \beta_T^0 \sqrt{1 - \beta_z^2}. \quad (5)$$

In the present model, the transverse radius of the fireball R formed in the most central collisions is assumed to decrease monotonically along the rapidity axis and is therefore written as

$$R = r_0 \exp\left(-\frac{z^2}{\sigma^2}\right), \quad (6)$$

where the parameter r_0 fixes the transverse size of the expanding hadronic matter at the freeze-out and σ represents the width of the matter distribution. By incorporating Eqs. (2)–(6), Eq. (1) takes the final form

$$\frac{d^2N}{2\pi p_T dp_T dy} = \frac{g}{(2\pi)^2} \times \int_{-\infty}^{\infty} \int_0^R \lambda E' \exp\left(-\frac{E'}{T}\right) r dr dz. \quad (7)$$

Integrating over p_T , we obtain the dN/dy yield from the above equation. In order to conserve the strangeness quantum number, we have used the criterion of the net strangeness equal to zero. The rest of the model details can be found in [5].

2. RESULTS AND DISCUSSION

The nuclear matter created in high-energy heavy ion collisions is assumed to form an ideal gas that can be described by the grand canonical ensemble. The density of the particle i can then be written as

$$n_i = \frac{g_i}{2\pi^2} \int_0^{\infty} \frac{k^2 dk}{\exp\left(\frac{E_i(k) - \mu_i}{T} \pm 1\right)}, \quad (8)$$

where $E_i = \sqrt{k^2 + m_i^2}$ is the energy and k is the momentum of the particle species. For high temperatures and energies, the Bose or Fermi–Dirac statistics can be replaced by the Boltzman statistics by dropping the ± 1 term. The chemical freeze-out relates with the equilibrium between different flavors. If the hadron gas reaches chemical equilibrium, the particle abundance is described by chemical potentials and temperatures. The information of the chemical freeze-out can be extracted from particle ratios in the measurement. Relative particle production can be studied by particle ratios of the integrated dN/dy yields. If we neglect the decay contributions and consider only the primordial yield, the like particle ratios are found to be controlled only by their respective fugacities:

$$\frac{n_i}{\bar{n}_i} = \exp\left(\frac{\mu_i - \bar{\mu}_i}{T}\right) = \exp\left(\frac{2\mu_i}{T}\right). \quad (9)$$

Ratios of particles with the same mass but different quark content, such as \bar{p}/p and k^-/k^+ , are sensitive to the balance between matter and antimatter, characterized by the baryon chemical potential μ_B . Because strange quarks are created during the collision and are not transported from the incoming nuclei, strangeness

Table. The chemical potential values obtained at different collision energies in our model are compared with the values obtained in Refs. [8, 9]

$\sqrt{s_{NN}}$	$\mu_B = a$, MeV; our model	μ_B , MeV; Refs. [8, 9]
9.2 GeV (SPS)	290 ± 3	300 ± 12
62.4 GeV (RHIC)	45 ± 5	62.7 ± 6
130 GeV (RHIC)	25 ± 3	29 ± 4.6
200 GeV (RHIC)	23 ± 2	22 ± 4.4
2.76 TeV (LHC)	0.5 ± 0.5	0.75

production is expected to be a good estimator of the degree of equilibration of the produced fireball [7]. The \bar{p}/p ratio in accordance with Eq. (9) can be written as

$$\frac{\bar{p}}{p} = \exp\left(-2\frac{\mu_B}{T}\right). \quad (10)$$

The other particle ratios can be correlated with the \bar{p}/p ratio as

$$\frac{k^-}{k^+} = \exp\left(2\frac{\mu_s}{T}\right) \left(\frac{\bar{p}}{p}\right)^{1/3}, \quad (11)$$

$$\frac{\bar{\Lambda}}{\Lambda} = \exp\left(-2\frac{\mu_s}{T}\right) \left(\frac{\bar{p}}{p}\right)^{2/3}, \quad (12)$$

$$\frac{\bar{\Sigma}}{\Sigma} = \exp\left(-2\frac{\mu_s}{T}\right) \left(\frac{\bar{p}}{p}\right)^{2/3}, \quad (13)$$

$$\frac{\bar{\Xi}}{\Xi} = \exp\left(-4\frac{\mu_s}{T}\right) \left(\frac{\bar{p}}{p}\right)^{1/3}, \quad (14)$$

$$\frac{\bar{\Omega}}{\Omega} = \exp\left(-6\frac{\mu_s}{T}\right). \quad (15)$$

Also, the energy dependence of the chemical potential can be approximated as [7]

$$\mu_B \propto \frac{1}{\sqrt{s_{NN}}}. \quad (16)$$

This energy dependence can also be verified from the different values of chemical potentials obtained in our previous papers [5] for different center-of-mass energies. These values along with the corresponding collision energies are given in Table. The uncertainties in these values of chemical potentials represent the uncertainties of the fit. For the sake of comparison, we mention the values of chemical potentials obtained at different SPS and RHIC energies by the STAR collaboration [8] and by ALICE at LHC [9].

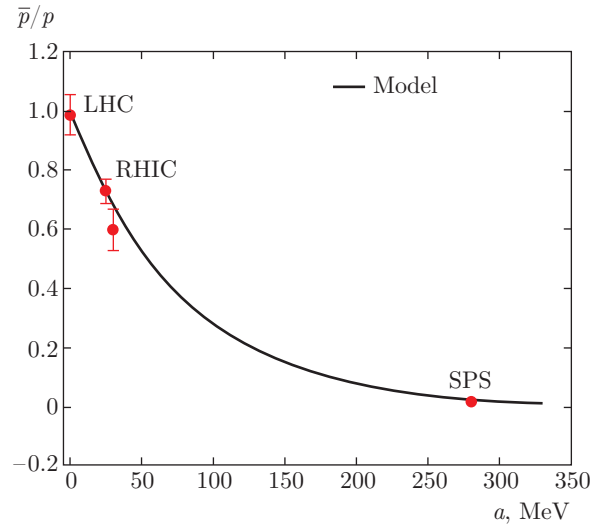


Fig. 1. \bar{p}/p ratio plotted as a function of the mid-rapidity chemical potential a . The SPS and RHIC data points are taken from [10] and the LHC data point is taken from [11, 12]

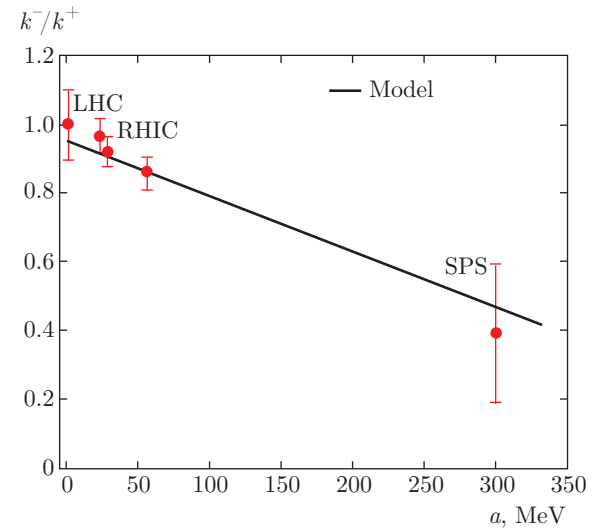


Fig. 2. k^-/k^+ ratio plotted as a function of the mid-rapidity chemical potential a . The SPS and RHIC data points are taken from [13] and the LHC data point is taken from [11, 12]

Thus, it is possible to replace the center-of-mass energy values with the values of the chemical potential and to reproduce and study the energy dependence of the various particle yield ratios by studying their dependence on the chemical potential. This is what we have done in the present analysis. We have extracted the various particle ratios with the help of Eqs. (10)–(15) and have plotted these ratios as a function of the mid-rapidity chemical potential ($\mu_B = a$) according to Eq. (2). We divide the chemical poten-

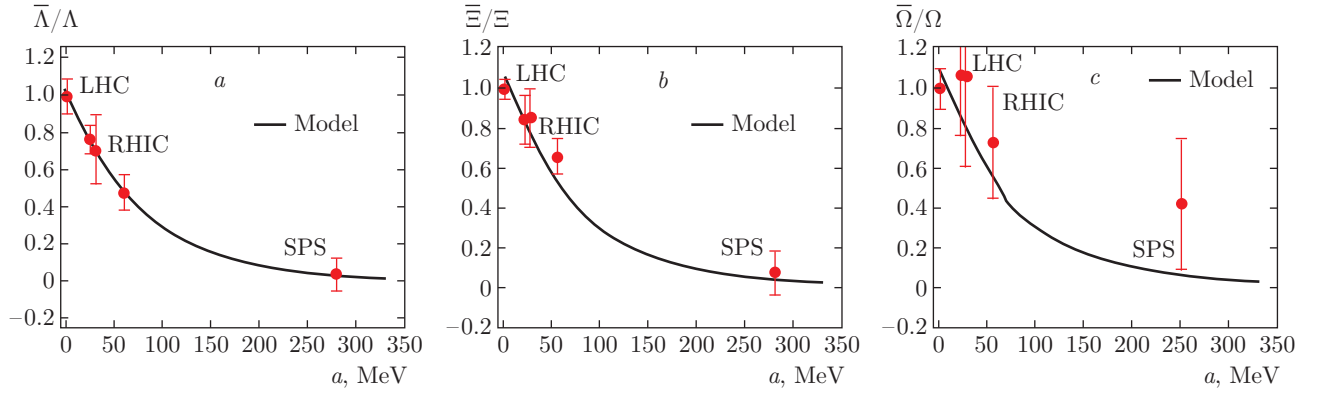


Fig. 3. $\bar{\Lambda}/\Lambda$ (a), $\bar{\Xi}/\Xi$ (b), and $\bar{\Omega}/\Omega$ (c) ratios plotted as functions of the mid-rapidity chemical potential a . The SPS and RHIC data points are taken from [14] and the LHC data point is taken from [11, 12]

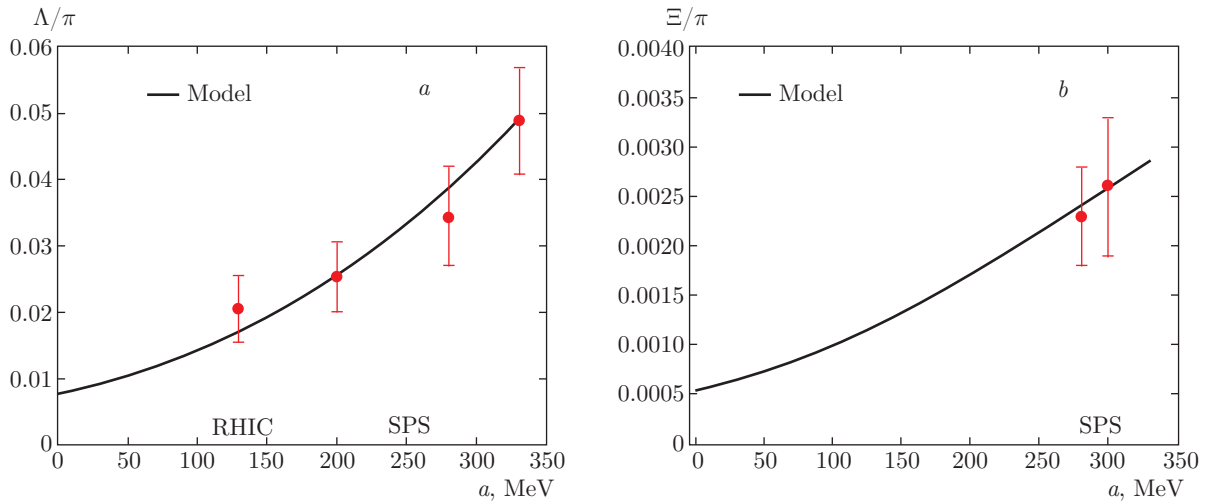


Fig. 4. Energy dependence of the Λ/π (a) and Ξ/π (b) ratios for central collisions at mid-rapidity

tial axis into three energy regimes of the SPS, RHIC, and LHC with reference to the values given in Table. Thus, the energy dependence of various particle ratios is established in this novel way. The newness of this approach is reflected in the successful reproduction of the particle ratios with respect to the collision energy and the chemical potential simultaneously.

In heavy-ion collisions, the increase in the antimatter-to-matter ratio with the center-of-mass energy of the system has been observed earlier by the NA49 and the STAR collaborations. The increase in the \bar{p}/p ratio toward unity with a decrease in the baryonic chemical potential and an increase in the center-of-mass energy from the SPS to the LHC is shown in Fig. 1. Our model results are in good agreement with the experimental data because our model curve reproduces the main features of the experimental data. The increase in the \bar{p}/p ratio with a decrease in the baryonic chemical poten-

tial and an increase in the collision energy reflects the decrease in the net baryon density towards higher collision energies, thus making the collision system partially transparent at the RHIC and almost completely transparent at the LHC energies. The ratio k^-/k^+ , plotted in Fig. 2, shows essential dependence on the center-of-mass energy. Our model prediction shows a close agreement with the experimental data points. Also the feature of the experimental curve is also in good agreement with our model calculations. The decrease in the k^-/k^+ ratio with an increase in the chemical potential and hence a decrease in the collision energy is due to an increase in the net baryon density, which leads to the associated production of kaons, thus favoring the production of k^+ over k^- .

In Fig. 3, we plot the energy dependence of strange and multi-strange antibaryon-to-baryon ratios. We find a fairly good agreement between our model results and

the experimental data. It is seen that the ratios increase towards unity with an increase in collision energies and with a decrease in the chemical potential. The ratios appear ordered with the strangeness quantum number, i. e., the higher the strangeness quantum number is, the smaller the difference between antibaryons and baryons. It is interesting to note that even the yield of very rarely produced strange particles like Ω is well described by the model. The particle ratios are found to be consistent with unity at the LHC, where the value of the chemical potential almost vanishes. This indicates the effects of complete nuclear transparency at the LHC.

We further reproduce the strange-to-nonstrange particle ratios as shown in Figs. 4 and 5. Unlike in the case of like particle ratios, here we include the effects of resonance decay contributions. Figure 6 shows the energy dependence of k^\pm/π^\pm ratios for central collisions at mid-rapidity. Our model results are in fair agreement with the experimental data points. At lower energies or higher chemical potentials, a peak has been observed in the k^+/π^+ ratio at around 8 GeV [15–17]. This is not reproduced in our analysis because of the invalidity of our approach at these lower energies, as is demonstrated in Fig. 5 in the case of the Ξ/π ratio. At very high chemical potentials or very low energies, our model could not reproduce the experimental data points. Thus, we have reproduced the results up to the SPS energy of 9.2 GeV only. However, the k^-/π^- ratio exhibits no sharp structure but a smooth evolution with the collision energy or the chemical potential. Also, the k^\pm/π^\pm ratio is seen to saturate at the RHIC and LHC energies. This saturation arises because of the freeze-out temperatures, which become constant at the RHIC and LHC energies. Although our model results for the k^-/π^- ratio are a little higher than the experimental data points, the main features of the data showing a steady decrease towards lower energies is well reproduced. The experimental data is taken from [17, 18]. Also in Fig. 4, we show the energy dependence of Λ/π and Ξ/π ratios. We find that our model results are in good agreement with the experimental data because our model curve reproduces the main features of the experimental data.

From the above particle ratios, we obtain the value of the chemical freeze-out temperature to be $169 \pm \pm 5$ MeV at the RHIC and LHC energies, while it shows a decreasing trend toward lower energies or higher chemical potentials and approaches a value of $150 \pm \pm 2$ MeV at the SPS energy of 9.2 GeV as shown in Fig. 7. The value of the chemical freeze-out temperature obtained at RHIC and LHC lies in the vicinity of

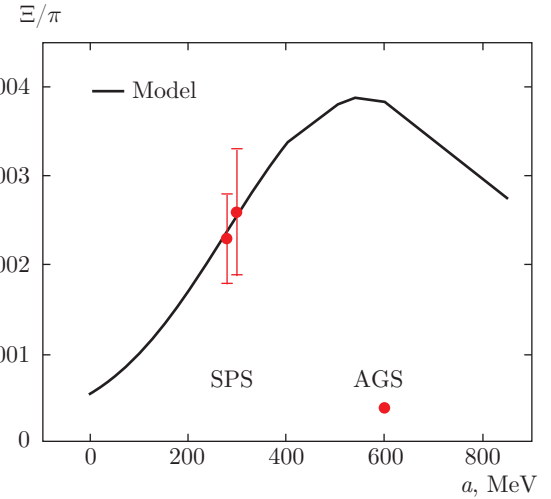


Fig. 5. Ξ/π ratio plotted as a function of the chemical potential a . The results are extrapolated to very low energies or very high chemical potentials

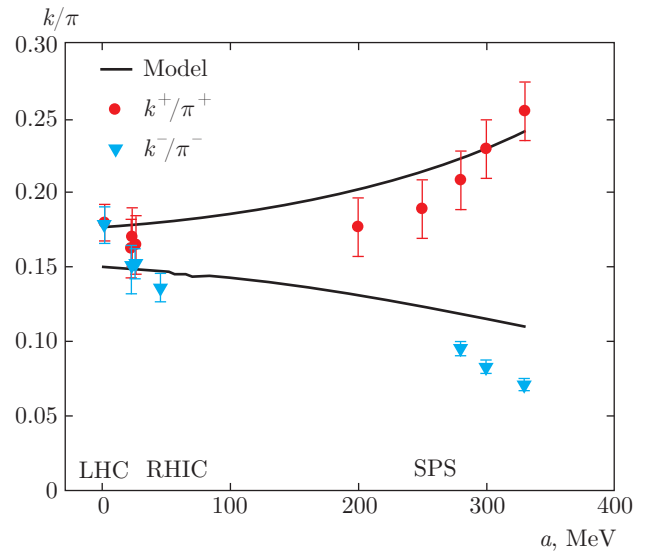


Fig. 6. Energy dependence of k^\pm/π^\pm ratios for central collisions at mid-rapidity

QCD-predicted phase transition temperature of around 170 MeV, indicating that the freeze-out occurs almost simultaneously after the phase transition.

The red filled squares in Fig. 7 represent the values of freeze-out temperatures obtained at the various collision energies mentioned in Table.

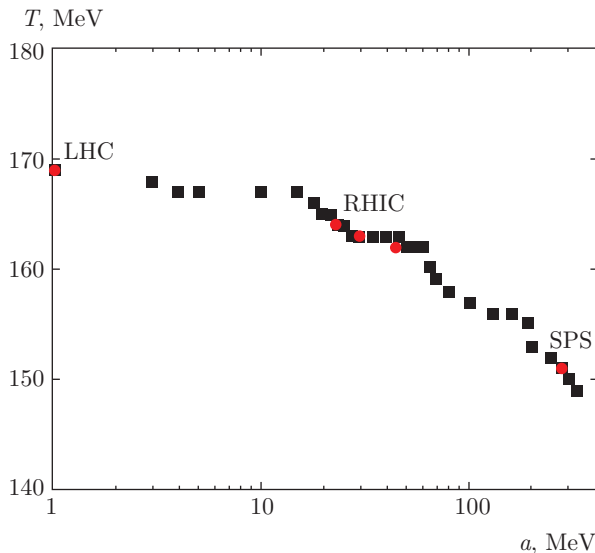


Fig. 7. (Color online). Chemical freeze-out temperature plotted as a function of the chemical potential

3. SUMMARY AND CONCLUSION

We have used our model to explain the variations of identified particle ratios with the mid-rapidity chemical potential and the center-of-mass energy simultaneously. An overall good agreement between our model results and experimental data supports the claim that the thermal model gives a satisfactory description of the data. The extracted value of the chemical freeze-out temperature is close to the lattice QCD-predicted phase-transition temperature, suggesting that chemical freeze-out happens in the vicinity of the phase boundary shortly after hadronization. The values of antiparticle-to-particle ratios are consistent with unity at the LHC energies (mid-rapidity chemical potential $a \approx 0$), thus indicating the effects of almost complete nuclear transparency in these collisions.

We acknowledge the financial support from University Grants Commission (UGC) for this work.

REFERENCES

1. U. W. Heinz, Nucl. Phys. A **661**, 140 (1999).
2. F. Becattini, Z. Phys. C **69**, 485 (1996); F. Becattini and U. Heinz, *ibid* **76**, 269 (1997); F. Becattini and G. Passaleva, Europ. Phys. J. C **23**, 551 (2002); F. Becattini, Nucl. Phys. A **702**, 336 (2002).
3. J. Cleymans and K. Redlich, Phys. Rev. Lett. **81**, 5284 (1998); J. Cleymans and K. Redlich, Phys. Rev. C **60**, 054908 (1999).
4. B. Biedron and W. Broniowski, Phys. Rev. C **75**, 054905 (2007).
5. S. Uddin et al., J. Phys. G **39**, 015012 (2012); S. Uddin et al., Nucl. Phys. A **934**, 121 (2015); S. Uddin et al., Adv. High Energy Phys. **2015**, 154853 (2015); Riyaz Ahmed Bhat et al., Nucl. Phys. A **935**, 43 (2015); Inam-ul Bashir et al., Int. J. Mod. Phys. A **30**, 1550139 (2015); S. Uddin et al., arXiv:1412.2663.
6. J. Cleymans, J. Phys. G: Nucl. Part. Phys. **35**, 044017 (2008); F. Becattini et al., Proc. Sci. CPOD07, 012 (2007).
7. O. Ristea, BRAHMS Collaboration, Rom. Rep. Phys. **56**, 659 (2004).
8. B. I. Abelev et al., STAR Collaboration, Phys. Rev. C **79**, 034909 (2009).
9. J. Cleymans, I. Kraus, H. Oeschler, K. Redlich, and S. Wheaton, Phys. Rev. C **74**, 034903 (2006).
10. B. B. Back et al., PHOBOS Collaboration, Phys. Rev. C **71**, 021901 (2005).
11. J. Cleymans, I. Kraus, H. Oeschler, K. Redlich, and S. Wheaton, Phys. Rev. C **74**, 034903 (2006).
12. A. Tawfik, E. Gamal, and A. G. Shalaby, Int. J. Mod. Phys. A **30**, 1550131 (2015).
13. B. I. Abelev et al., STAR Collaboration, Phys. Rev. C **79**, 034909 (2009).
14. M. M. Aggarwal et al., STAR Collaboration, Phys. Rev. C **83**, 024901 (2011).
15. P. Braun-Muzinger, J. Cleymans, H. Oeschler, and K. Redlich, Nucl. Phys. A **697**, 902 (2002).
16. J. Cleymans, H. Oeschler, K. Redlich, and S. Wheaton, Phys. Lett. B **615**, 50 (2005).
17. M. Mishra and C. P. Singh, Phys. Rev. C **78**, 024910 (2008).
18. C. Blume et al., NA49 Collaboration, J. Phys. G **31**, S685 (2005).